Available online at www.sciencedirect.com
ScienceDirect
Journal of Power Sources 164 (2007) 372–378
JOURNAL OF POWER SOURCES
www.elsevier.com/locate/jpowsour

Electrochemical studies of low-temperature processed nano-crystalline $LiMn_2O_4$ thin film cathode at 55 °C

S.B. Tang, M.O. Lai, L. Lu *

Department of Mechanical Engineering, National University of Singapore, 117576 Singapore, Singapore

Received 19 July 2006; received in revised form 24 August 2006; accepted 15 September 2006
Available online 22 November 2006

Abstract

$LiMn_2O_4$ thin films with nano-crystals less than 100 nm were successfully grown on polished stainless steel substrates at 400 °C and 200 m Torr of oxygen by pulsed laser deposition. A maximum discharge capacity of 62.4 μAh cm^{-2} μm^{-1} cycled between 3.0 and 4.5 V with a current density of 20 μAh cm^{-2} was achieved. The effect of several overdischarge cycles was negligible, and both the effect of Jahn–Teller distortion at low potentials on capacity loss and structure instability at high potentials were effectively inhibited in this nano-crystalline film, resulting in an excellent cycling stability with a very low fading rate of capacity up to 500 cycles at 55 °C.

Keywords: Nano-crystalline $LiMn_2O_4$ thin film; Pulsed laser deposition; Capacity; Charge/discharge; Stability

1. Introduction

Spinel $LiMn_2O_4$ has been proposed as a cathode material for rechargeable batteries and studied for many years. Cubic $LiMn_2O_4$ can reversibly insert Li^+ in 3 V plateau and extract Li^+ in 4 V process. Compared to commonly used $LiCoO_2$, the advantages of $LiMn_2O_4$ include high potential, low cost and low toxicity [1]. However, its application in commercial batteries is very limited due to the significant capacity decay of bulk materials in storage and extended cycling, especially at the elevated temperatures. There are several suggested factors possibly leading to the capacity fading: (i) Jahn–Teller effect in 3 V plateau involving in the structure distortion from cubic to tetragonal phase transformation [2,3]; (ii) the dissolution of manganese into the electrolyte through the disproportion reaction: $2Mn^{3+} \rightarrow Mn^{2+} + Mn^{4+}$ [4]; (iii) the transformation of the unstable two-phase structure at high potentials to a more stable single-phase structure via the loss of MnO [5,6]. In order to improve the electrochemical performance of spinel $LiMn_2O_4$, substituting for manganese with other elements [7–10] and coating the surfaces of $LiMn_2O_4$ with various oxides and protective films [11–13] have been investigated.

Besides the usage in volume batteries, thin film $LiMn_2O_4$ may be used as a cathode in microbatteries that have attracted more interest in recent years [14]. $LiMn_2O_4$ thin films have been grown using electrostatic spray deposition (ESD) [15–18], electron-beam evaporation [19], radio frequency (rf) sputtering [20,21] and pulsed laser deposition (PLD) [22–25]. However, most of the previous studies have been focused on the electrochemical properties of high-temperature processed $LiMn_2O_4$ thin films mainly measured at room temperature. Mohamedi et al. [26] recently investigated the effect of three different liquid electrolytes ($LiClO_4$, $LiBF_4$ and $LiPF_6$) on the electrochemical stability of thin film $LiMn_2O_4$ prepared by ESD and observed that the $LiPF_6$ electrolyte caused the fastest fading of capacity at 55 °C. Shu et al. [12] recently found that $LiCoO_2$-coated $LiMn_2O_4$ film greatly improved cycling stability at 55 °C though it still showed a decay rate of about 0.22% per cycle up to 50 cycles, measured between 3.5 and 4.35 V. Here, we reported the excellent electrochemical properties of pure nano-crystalline $LiMn_2O_4$ thin films that were developed by low-temperature processed PLD and measured in a wide potential range of 3–4.5 V at 55 °C.

2. Experimental

$LiMn_2O_4$ thin films were deposited on stainless steel substrates (polished by 0.3 μm alumina) by PLD. A focused excimer

* Corresponding author. Tel.: +65 65162236; fax: +65 6779 1459.
E-mail address: luli@nus.edu.sg (L. Lu).

0378-7753/$ – see front matter © 2006 Elsevier B.V. All rights reserved.
doi:10.1016/j.jpowsour.2006.09.109

laser beam (248 nm, KrF) with power of 160 mJ per pulse and frequency of 10 Hz was used to irradiate a $LiMn_2O_4$ target supplied by SCI Engineered Materials Inc. (USA). The base pressure of the vacuum chamber was 2×10^{-5} Torr. The distance between target and substrate was kept at 4 cm and the target was rotated during the film growth. The films were deposited in pairs, one on Si substrate for the cross-sectional SEM measurement whereas the other one on stainless steel substrate for electrochemical test and other characterizations. The film was deposited for 40 min at 400 °C and 200 m Torr of oxygen, under which conditions the film deposited was mainly composed of nano-crystals less than 100 nm as observed by AFM.

Surface topography and roughness of the as-deposited films were characterized using an atomic force microscope (AFM, SPI 3800N, Seiko Instruments Inc.), operating in a dynamic mode. Thickness of the film was estimated by cross-sectional SEM of the film deposited on Si substrate (Hitachi 4100 field-emission scanning electron microscope). Crystalline structure of films was characterized using a Shimadzu XRD-6000 diffractometer with a Cu Kα source. Raman spectroscope measurements were carried out using a Jobin-Yvon T64000 micro-Raman system equipped with a charge-coupled device (CCD) detector. Samples were excited by the polarized 514.5 nm line of Ar^+ laser at a power level of 5 mW. The laser spot size at the surface of the sample is about 1 μm and the spectrum resolution is about 0.5 cm^{-1}.

An electrochemical cell was assembled into a home-made Swagelok cell using a $LiMn_2O_4$ film of 10 mm diameter as cathode and Li metal foil as anode electrode. The assembly was carried out in an Ar-filled glove box with both H_2O and O_2 levels less than 0.1 ppm. The electrolyte is 1 M $LiPF_6$ in 1:1 ethylene carbonate (EC) and diethyl carbonate (DEC) solution. Electrochemical measurements were performed at 55 ± 2 °C using a Solartron 1287 electrochemical interface and 1260 frequency response analyzer. Charge and discharge tests were performed between 3.0 and 4.5 V, under constant current densities. Cyclic voltammetry (CV) was scanned in the potential range of 3.5–4.5 V for the normal scan and in the range of 2.0–4.5 V for the overdischarge scan at a sweep rate of 0.2 mV/s. Electrochemical impedance spectroscopy (EIS) was conducted in a frequency range from 300 kHz to 0.005 Hz using an AC signal with amplitude of 10 mV.

3. Results and discussion

Fig. 1 shows the change of discharge capacity with cycle numbers cycled between 3.0 and 4.5 V at 55 °C. The initial discharge capacity was about 59.6 μAh cm^{-2} μm with a current density of 20 μAh cm^{-2}. A maximum capacity of 62.4 μAh cm^{-2} μm^{-1} at around seventh cycle was achieved and it then decayed at an average rate of 0.078% per cycle up to 100 cycles. In order to examine its long-term stability, the film was continuously cycled at higher current densities of 100 μAh cm^{-2} from 101 to 500 cycles, in which it showed an average capacity loss rate of 0.07% per cycle. In general, the capacity loss exacerbates with the increase in charge/discharge current density. When the current density was increased five times after 100 cycles, the

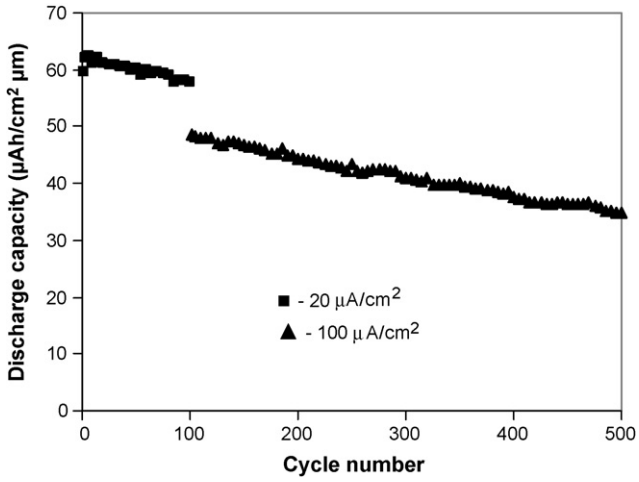

Fig. 1. Change in discharge capacity with cycle numbers of nano-crystalline $LiMn_2O_4$ film on stainless steel substrate at 55 °C (current density is 20 μA cm^{-2} for the first 100 cycles and 100 μA cm^{-2} from cycle 101 to 500).

fading rate was observed to be even slightly lower, indicating that the film with a nano-crystalline structure exhibited excellent cycling stability and capacity retention and could effectively overcome the unstable factors in $LiMn_2O_4$ cathode material to a great extent [2–6]. The charge and discharge curves at different cycles and with different current densities are shown in Fig. 2. Two typical and a little smooth plateaus at about 4.0 and 4.15 V were observed. It also showed some discharge capacity between 3.0 and 3.3 V, which may be related to the 3 V processes of $LiMn_2O_4$ that will be discussed later. By comparing the charge/discharge curves between cycle 100th and 101st, it can be seen that with the increase in current density the charge cell voltage was raised while the discharge cell voltage was lowered. This is most likely caused by the increased cell polarization arising from Li-ion diffusion process in the cathode [25]. About 15.9%

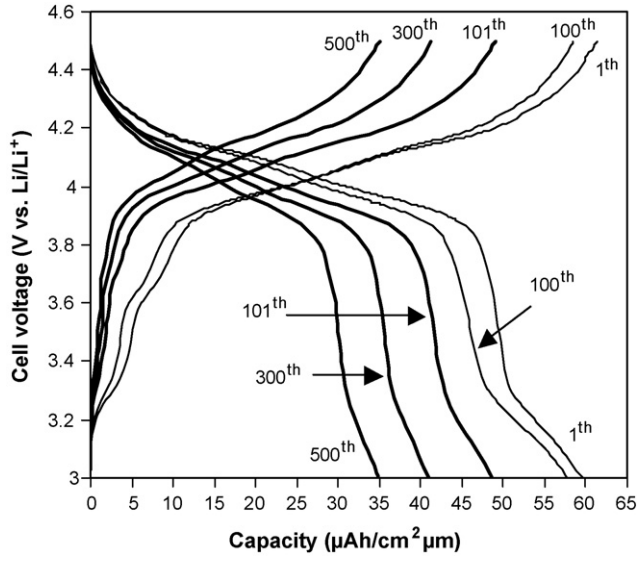

Fig. 2. Charge/discharge curves of $LiMn_2O_4$ film cathode in different number of cycles at 55 °C (current density is 20 μA cm^{-2} for the 1st and 100th cycles and 100 μA cm^{-2} for 101st, 300th and 500th cycles).

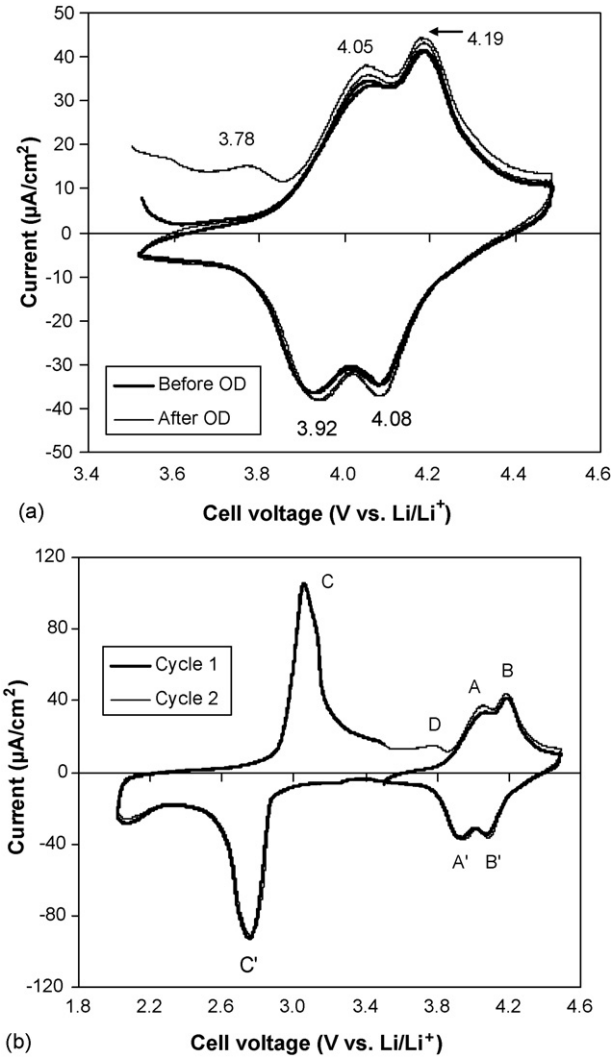

Fig. 3. Cyclic voltammogram of nano-crystalline $LiMn_2O_4$ film electrode at 55 °C and a scan rate of 0.2 mV s^{-1}: (a) the normal scans from 3.5 to 4.5 V before and after overdischarge scan; (b) overdischarge scan down to 2.0 V (OD—overdischarge).

of drop in discharge capacity was observed when the current density was increased from 20 to 100 μAh cm^{-2}. Striebel et al. found 54% of capacity drop in their highly crystallized $LiMn_2O_4$ film grown by PLD as the current density was increased from 10 to 100 μAh cm^{-2} [22]. The charge/discharge curves in the 500th cycle were similar to those in the 101st, the initial cycle using the same current density of 100 μAh cm^{-2}, though the plateaus became short due to the gradual fading of capacity.

Fig. 3 presents the cyclic voltammogram of $LiMn_2O_4$ film measured after 10 charge/discharge cycles at 55 °C, with a sweep rate of 0.2 mV s^{-1}. For the normal scan from 3.5 to 4.5 V (Fig. 3a), the film shows two pairs of broad peaks located at 3.92, 4.05, 4.08 and 4.19 V, corresponding to two plateaus of charge/discharge curves in Fig. 2 and two-step reversible (de)intercalation of lithium ions between $LiMn_2O_4$ and λ-MnO_2 [22]. The second CV curve well overlaps with the first, further confirming good cycling repeatability of the film. The film was then overdischarged (OD) down to 2 V to investigate the effect of overdischarge that may cause serious capacity fading due to Jahn–Teller distortion in 3 V process [2,3,27]. The Jahn–Teller effect is symmetry-lowered distortion that splits the electronic ground state degeneracy, leading to a lower symmetry in individual coordination polyhedra. As shown in Fig. 3b, besides the previous two pairs of peaks for the 4 V process (denoted as A and B), there observed a pair of strong peaks (denoted as C and C′) located at 3.05 V on charge and 2.75 V on discharge. This pair of peaks clearly represents the 3 V process, corresponding to the insertion/extraction of lithium between cubic $LiMn_2O_4$ and tetragonal $Li_2Mn_2O_4$. More than 50% Jahn–Teller ions (Mn^{3+}) presented in $Li_2Mn_2O_4$ produces the cubic to tetragonal distortion. This phase transformation results in about 6% volume change in a unit cell that imparts a high degree of stress in grains. With the repeating insertion/extraction of Li^+ in 3 V process, grain fracture may occur. The fractured grains may not be accessible anymore for Li^+, resulting in the capacity loss finally [2,3,27]. One new and weak peak denoted as D at around 3.78 V appeared in the second charge scan, possibly from the further deintercalation of lithium that was not fully removed in the 3 V process due to the structure disorder. All other sections in two continuous scans well overlapped to each other. After two overdischarge CV scans, two normal CV scans from 3.5 to 4.5 V and then charge/discharge test from 3 to 4.5 V were performed. The oxidation/reduction peaks in 4 V process could be almost recovered from the overdischarge and no capacity fading was observed (see Fig. 3a after OD). The charge/discharge cycling test measured between 3 and 4.5 V before and after overdischarge CV scans further confirmed no obvious capacity loss. There is thus no harmful effect from several overdischarge scans in the present nano-crystalline $LiMn_2O_4$ film at 55 °C, compared to that in the highly crystallized film as studied at room temperature by Rougier et al. [27] who found that the capacity associated to 3 V process was much lower (<1/3) than that of 4 V process. After overdischarge CV scans, 20% of

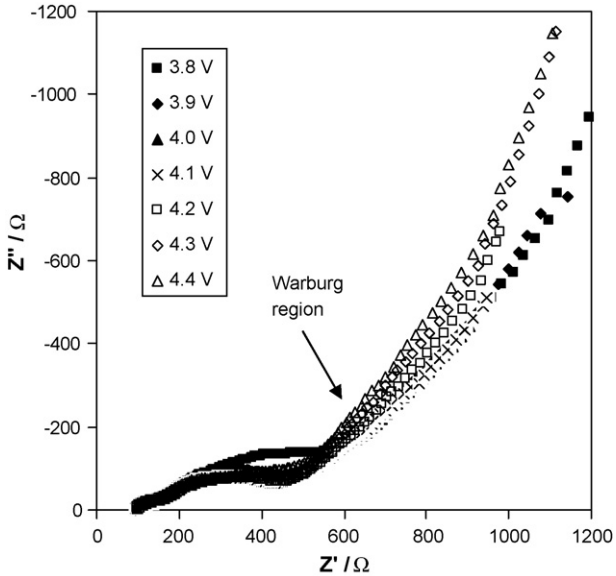

Fig. 4. AC impedance spectra of $LiMn_2O_4$ thin film at 55 °C and several different potentials between 3.8 and 4.4 V.

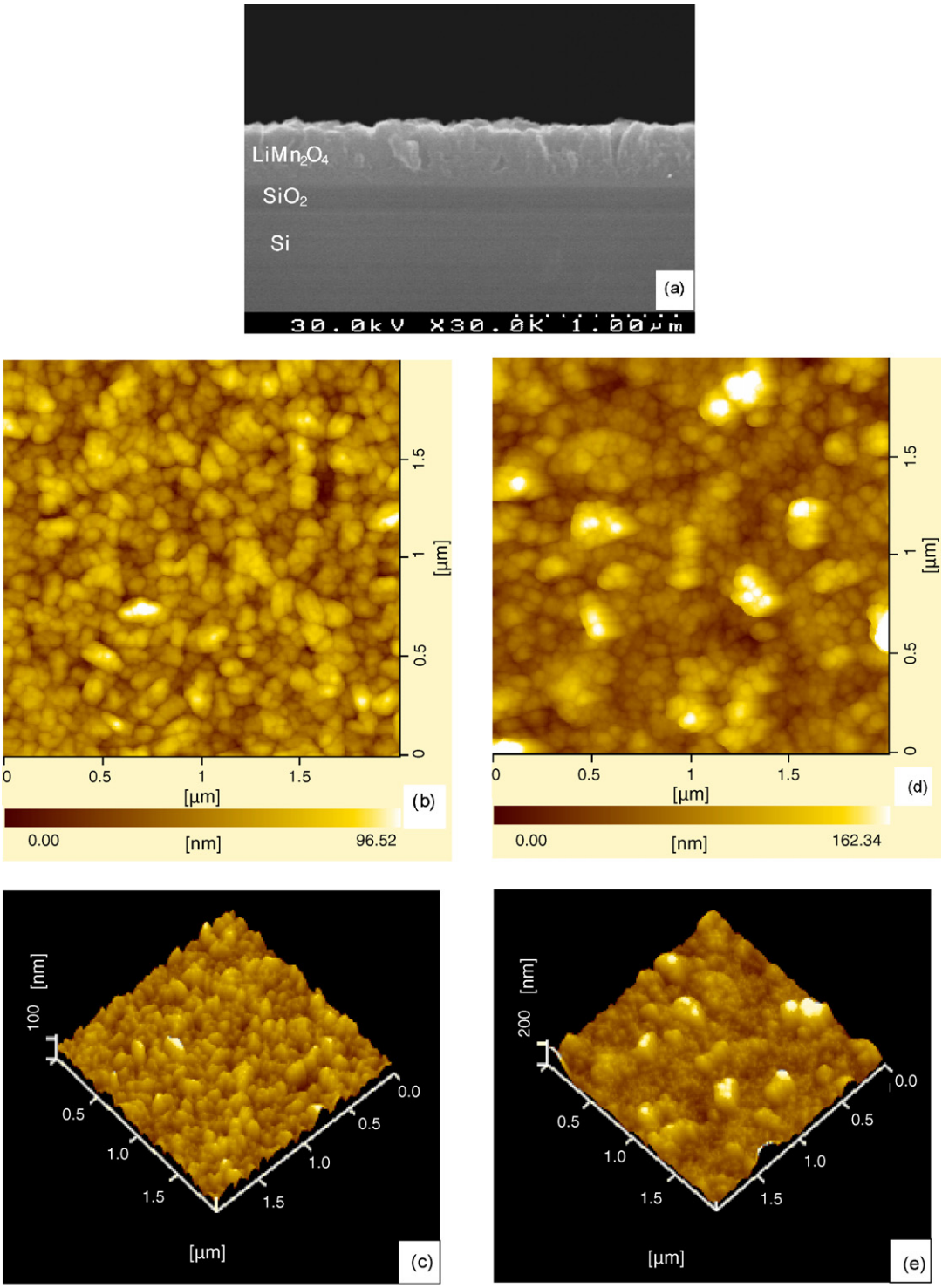

Fig. 5. Cross-sectional SEM of the as-deposited film on Si substrate at 400 °C and 200 m Torr of oxygen (a) and AFM surface topography of the $LiMn_2O_4$ thin film grown on stainless steel substrates: (b) flat image of the as-deposited, (c) 3D image of the as-deposited film, (d) flat image and (e) 3D image of the cycled film after 500 cycles at 55 °C.

capacity loss in charge/discharge test between 3.5 and 4.35 V was observed in their film. John–Teller distortion seems serious in highly crystallized film or powder with large crystals that may be more easily fractured to produce electrically isolated particles. Therefore, the effect of Jahn–Teller distortion related to Mn^{3+} ion that is claimed to lead to the capacity loss in $LiMn_2O_4$ is not obvious in the present nano-crystalline film, at least in several cycles.

Fig. 4 shows the AC impedance spectra of the film in the potential range of 3.8–4.4 V measured at 55 °C. Each Nyquist plot is composed of deformed semicircle region in high and medium frequencies and a Warburg region followed by a steep

sloping line at the lowest frequencies. The semicircle region in the high- and medium-frequencies can be fitted into two semicircles using an equivalent circuit similar to the model in reference [16]. The first small semicircle in the high-frequency may be attributed to the surface film formed on the $LiMn_2O_4$ electrode by electrolyte solution (with a resistance of ~85 Ω). The second large semicircle in the medium frequency is dependant on potentials and thus ascribed to the interfacial Li-ion transfer resistance (R_{CT}). It can be observed that the charge-transfer resistance decrease slightly with the increase of potentials from about 360 Ω at 3.80 V to 260 Ω at 4.0 V and then there is almost no obvious change up to 4.4 V. This change trend of Li-ion charge-transfer resistance with potentials is significantly different from that in highly crystallized $LiMn_2O_4$ film electrodes reported by Yamada et al. [24] who observed a minimum resistance at around 3.96 V and a continuous increase of the resistance over 4.0 V, especially a much high resistance value at 4.2 V. The change of R_{CT} with potentials may be related to the structure change of $LiMn_2O_4$ with the removal of Li^+ [12]. The more structure change may occur in highly crystallized film composed of big crystals at high potentials whereas nano-crystals show less change and better stability in structure. Additionally, the Warburg region is closely related to the Li^+-ion diffusion. The chemical diffusion coefficient for the finite-space solid-state diffusion can be estimated from the Warburg slope of the straight line section in the Warburg region, $A_w = \Delta Re/\Delta\omega^{-1/2} = \Delta Im/\Delta\omega^{-1/2}$, where ΔRe and ΔIm are the differences between the real and imaginary components of the AC impedance corresponding to a finite change in angular frequency, $\Delta\omega$. The Warburg slope can be derived from Fick's law as follows [28]:

$$A_w = \frac{(dE/dx)}{V_m/(\sqrt{2D}zFA)} \quad (1)$$

where dE/dx is the slope of the electrode potential (E) curve versus x in $Li_xMn_2O_4$, V_m the molar volume of $LiMn_2O_4$, D the diffusion coefficient of Li^+-ion ($cm^2\ s^{-1}$), z the charge-transfer number, F the Faraday constant and A is the area of electrode (cm^2). The dE/dx values at various potentials can be derived from the discharge curves under a constant current density (Fig. 2). The calculated diffusion coefficients of Li^+-ion at 55 °C were around $2.7 \times 10^{-12}\ cm^2\ s^{-1}$ for 4.0 V and $2.4 \times 10^{-11}\ cm^2\ s^{-1}$ for 4.2 V, which are lower than the reported values in the $LiMn_2O_4$ thin film prepared by ESD (in the range of 10^{-12} to $10^{-9}\ cm^2\ s^{-1}$ at room temperature [16] and 10^{-10} to $10^{-9}\ cm^2\ s^{-1}$ at 55 °C depending on the potentials [26]) and the values at room temperature in highly crystallized $LiMn_2O_4$ thin film grown by PLD ($1.9 \times 10^{-11}\ cm^2\ s^{-1}$ at 3.5 V and $2.3 \times 10^{-10}\ cm^2\ s^{-1}$ at 4.5 V) [29]. This difference in diffusion coefficients may be related to different properties between the films, such as morphology, crystallization and crystal sizes.

AFM, XRD and Raman were used to examine the film properties before and after electrochemical cycling. Fig. 5 shows the cross-sectional SEM image of $LiMn_2O_4$ thin film on Si substrate and surface topography (measured by AFM) on stainless steel substrates grown at 400 °C and 200 mTorr of oxygen. The cross-sectional SEM image shows a dense $LiMn_2O_4$ film (Fig. 5a). The as-deposited film is mainly consisted of nano-crystals less than 100 nm and their agglomerates (Fig. 5b). The root mean square (rms), roughness of the film, is about 15.2 nm. After 500 cycles of charge/discharge test at 55 °C, most of nano-grains remained unchanged. However, some large agglomerates were formed and observed on the surface, which increased the roughness of the film with rms of about 28.8 nm (Fig. 5d). This may be due to the electrochemical migration and agglomeration of small nano-grains during cycling as also observed on nano-sized alloy anodes [30].

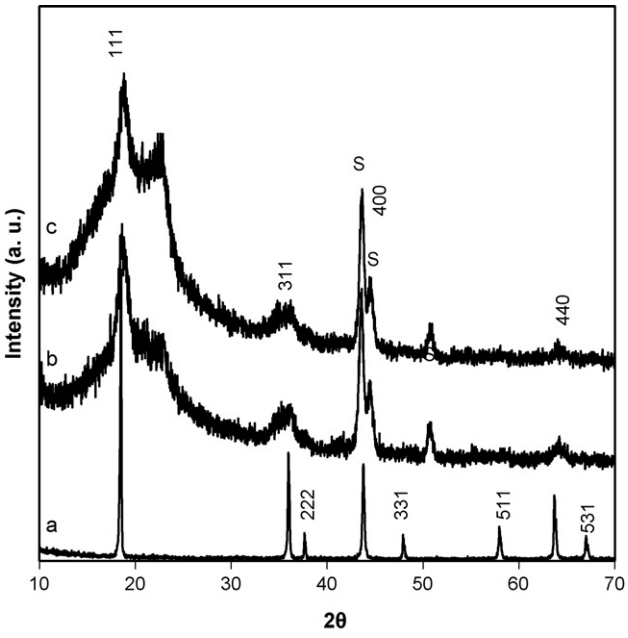

Fig. 6. XRD patterns of $LiMn_2O_4$ target (a) and nano-crystalline thin films of (b) in the as-deposited and (c) after 500 cycles between 3.0 and 4.5 V at 55 °C (S—substrate).

Fig. 6 shows XRD patterns of $LiMn_2O_4$ target and films on stainless steel substrates in the as-deposited and after 500 cycles of charge/discharge at 55 °C. The target showed strong and narrow peaks (Fig. 6a), typical of highly crystallized spinel $LiMn_2O_4$. In the as-deposited nano-crystalline film (Fig. 6b), a relatively stronger and broad diffraction peak (1 1 1) at 2θ of 18.7° was observed. Other two weak peaks of (3 1 1) and (4 4 0) could be detectable. The peak (4 0 0) was overlapped with the substrate and hence could not be distinguished. Compared to the highly crystallized target, the main peak of (1 1 1) in thin film was much broad and shifted into a little higher degree. The weak peaks of (2 2 2), (3 3 1), (5 1 1) and (5 3 1) were not detected. These are mainly due to small size of crystals and low crystallization in nano-crystalline film as usually observed in nano-materials. However, the main XRD features of the film are in line with of regular spinel $LiMn_2O_4$. After 500 charge/discharge cycling test between 3.0 and 4.5 V (Fig. 6c), the main peak positions remained at the same 2θ values. Raman spectra of the as-deposited and cycled $LiMn_2O_4$ films on stainless steel substrates are shown in Fig. 7. For the as-deposited film (Fig. 7a), a strong band centered at 651 cm^{-1} and a weak

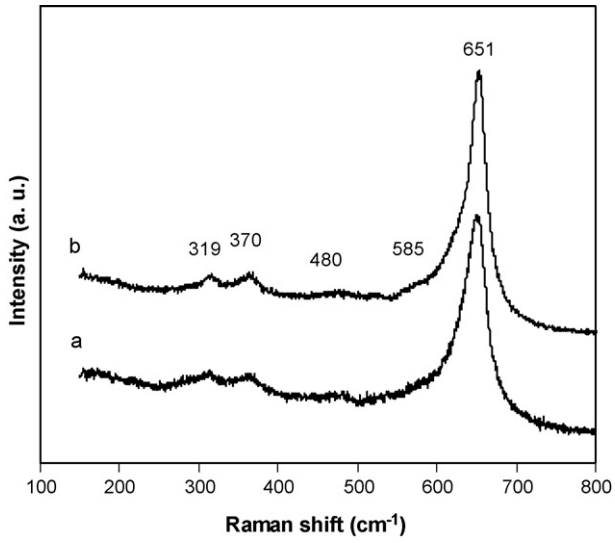

Fig. 7. Raman spectra of $LiMn_2O_4$ thin films of (a) in the as-deposited and (b) after 500 cycles between 3.0 and 4.5 V at 55 °C.

shoulder located at 585 cm^{-1} were detected. Three very weak and broad bands at about 480, 370 and 319 cm^{-1} were also observable. The strong band at 651 cm^{-1} is attributed to A_{1g} mode, corresponding to the symmetric Mn–O stretching vibration of MnO_6 groups while the peaks located at 585, 480 and 370 cm^{-1} may be assigned to three modes of T_{2g} phonons [31]. The weak peak of 319 cm^{-1} is not very clear. The Raman spectra of $LiMn_2O_4$ are complicated and the assignments are not unambiguous since sometimes there appeared more number of vibrations than that predicated by group theory for the perfect spinel compound with *Fd3m* symmetry [31]. Raman spectra of $LiMn_2O_4$ have some change from process to process due to varying degrees of disorder in reality [21,31]. As shown in Fig. 7b, after 500 cycles of charge/discharge the Raman characteristics were kept almost unchanged, revealing the stability of microstructures in this nano-crystalline film after long-term cycling.

The present nano-crystalline $LiMn_2O_4$ film grown at a low-temperature possesses the three-dimensional networks for Li-ion diffusion. The very small grains and high effective surface area will facilitate lithium diffusion into and out of crystals. Xia et al. [6] suggested that the transformation of an unstable two-phase to a more stable one-phase structure takes place during the extraction/insertion of Li^+ ions at high potentials, which is accompanied by the loss of MnO with cycling leading to the capacity fading. With the extraction of lithium ions, the original $LiMn_2O_4$ transforms to λ-MnO_2. During the charge and discharge cycling the total volume change (shrinkage and expansion) in small crystals should be smaller and the stress caused within the crystals with the Li-ion insertion/desertion is thus expected to be smaller. This is supported by the low charge-transfer resistances at high potentials above 4 V. Compared to the powder $LiMn_2O_4$ electrode that contains organic binder and conductive carbon, thin film electrode, especially nano-crystalline film, is more dense and compact with smaller interstices between particles. The dissolution of manganese into liquid electrolyte can be weakened to some extent. The nano-crystalline film can effectively inhibit both Jahn–Teller distortion in 3 V process and structure instability in 4 V process, and thus exhibited very low fading rate of capacity. The main factor leading to the capacity loss may be the gradual manganese dissolution induced by HF due to the electrochemical decomposition of electrolyte at elevated temperatures [12]. It is thus expected that the electrochemical stability of the present nano-crystalline $LiMn_2O_4$ film in all-solid microbatteries should be better.

4. Conclusions

Nano-crystalline $LiMn_2O_4$ film cathode developed at low temperatures by PLD exhibited a maximum capacity of 62.4 μAh cm^{-2} μm^{-1} cycled between 3.0 and 4.5 V with a current density of 20 μAh cm^{-2} and a good capacity retention up to 500 cycles at elevated temperatures, bringing promising prospect in practical application as a thin film cathode in microbatteries.

Nano-crystalline $LiMn_2O_4$ film possesses three-dimensional networks for Li-ion diffusion and its small grains and high effective surface area have confirmed to facilitate lithium diffusion into and out of crystals and thus benefits capacity retention by preventing both the damage of Jahn–Teller effect at low voltages and structure instability at high voltages as revealed by overcharge test and AC impedance spectra, respectively. Raman spectra and XRD results confirmed the stable structure of this nano-crystalline $LiMn_2O_4$ film after a long-term cycling test at 55 °C.

Acknowledgements

This work has been supported by the National University of Singapore under research grants R265-000-133-112 and R265-000-162-112.

References

[1] M. Broussely, P. Biensan, B. Simon, Electrochim. Acta 45 (1999) 3.
[2] M.M. Thackeray, W.I.F. David, P.G. Bruce, J.B. Goodenough, Mater. Res. Bull. 18 (1983) 461.
[3] S.J. Wen, T.J. Richardson, L. Ma, K.A. Striebel, P.N. Ross Jr., E.J. Cairns, J. Electrochem. Soc. 143 (1996) 136.
[4] H. Kanoh, Q. Feng, T. Hirotsu, K. Ooi, J. Electrochem. Soc. 143 (1996) 2610.
[5] V. Manev, B. Banov, A. Momchiler, A. Nassalevska, J. Power Sources 57 (1995) 99.
[6] Y. Xia, Y. Zhou, M. Yoshio, J. Electrochem. Soc. 144 (1997) 2593.
[7] L. Guohua, H. Ikuta, T. Uchida, M. Wakihara, J. Electrochem. Soc. 143 (1996) 178.
[8] A. Antonini, C. Bellitto, M. Pasquali, G. Pistoia, J. Electrochem. Soc. 145 (1998) 2726.
[9] H.S. Moon, J.W. Park, J. Power Sources 119 (2003) 717.
[10] M. Hosoya, H. Ikuta, M. Wakihara, Solid State Ionics 111 (1998) 153.
[11] Z. Zheng, Z. Tang, Z. Zhang, W. Shen, Y. Lin, Solid State Ionics 148 (2002) 317.
[12] D. Shu, G. Kumar, K.B. Kima, K.S. Ryub, S.H. Chang, Solid State Ionics 160 (2003) 227.
[13] H.S. Moon, S.W. Lee, Y.K. Lee, J.W. Park, J. Power Sources 119 (2003) 713.

[14] K.-L. Lee, J.-Y. Jung, S.-W. Lee, H.-S. Moon, J.-W. Park, J. Power Sources 130 (2004) 241.
[15] A.A. Van Zomeren, E.M. Kelder, J.C.M. Marijnissen, J. Schoonman, J. Aerosol Sci. 25 (1994) 1229.
[16] M. Mohamedi, D. Takahashi, T. Uchiyama, T. Itoh, M. Nishizawa, I. Uchida, J. Power Sources 93 (2001) 93.
[17] M. Mohamedi, D. Takahashi, T. Itoh, M. Umeda, I. Uchida, J. Electrochem. Soc. 149 (2002) A19.
[18] J.L. Shui, G.S. Jiang, S. Xie, C.H. Chen, Electrochim. Acta 49 (2004) 2209.
[19] M.M. Thackeray, J. Electrochem. Soc. 144 (1997) L100.
[20] T. Brousse, P. Fragnaud, R. Marchand, D.M. Schleich, O. Bohnke, A.K. West, J. Power Sources 68 (1997) 412.
[21] K.F. Chiu, H.C. Lin, K.M. Lin, C.H. Tsai, J. Electrochem. Soc. 152 (2005) A2058.
[22] K.A. Striebel, C.Z. Deng, S.J. Wen, E.J. Cairns, J. Electrochem. Soc. 143 (1996) 1821.
[23] M. Morcrette, P. Barboux, J. Perriere, T. Brousse, A. Traverse, J.P. Boilot, Solid State Ionics 138 (2001) 213.
[24] I. Yamada, T. Abe, Y. Iriyama, Z. Ogumi, Electrochem. Commun. 5 (2003) 502.
[25] C. Julien, E. Haro-Poniatowski, M.A. Camacho-Lopez, L. Escobar-Alarcon, J. Jimenez-Jarquin, Mater. Sci. Eng. B 72 (2000) 36.
[26] M. Mohamedi, D. Takahashi, T. Itoh, I. Uchida, Electrochim. Acta 47 (2002) 3483.
[27] A. Rougier, K.A. Striebel, S.J. Wen, E.J. Cairns, J. Electrochem. Soc. 145 (1998) 2975.
[28] C. Ho, I.D. Raistrick, R.A. Huggins, J. Electrochem. Soc. 127 (1980) 343.
[29] K.A. Striehel, A. Rougier, C.R. Horne, R.P. Reade, E.J. Cairns, J. Electrochem. Soc. 146 (1999) 4339.
[30] S.-W. Song, K.A. Striebel, R.P. Reade, G.A. Roberts, E.J. Cairns, J. Electrochem. Soc. 150 (2003) A121.
[31] B. Ammundsen, G.R. Burns, M.S. Islam, H. Kanoh, J. Roziere, J. Phys. Chem. B 103 (1999) 5175.